Supplementary Information

Enhanced methanol oxidation performance on platinum with butterfly-scale architectures: toward structural design of efficient electrocatalysts

Xingmei Guo, Han Zhou, Di Zhang, and Tongxiang Fan*

State Key Lab of Metal Matrix Composites, Shanghai Jiaotong University, 800 Dongchuan Road, Shanghai, 200240, China. E-mail: txfan@sjtu.edu.cn; Fax: +86-21-34202749; Tel: +86-21-54747779

Contents

S1. Platinum synthesis

Template samples: Butterfly wings are arranged like roof-tiles with a flat membrane covered by scales on both the dorsal and ventral side. Here, we chose the blue scales of *Morph* butterfly wings, yellow scales of *Troides aeacus* butterfly hind-wings, and black scales of *Troides aeacus* butterfly fore-wings as templates to synthesize *lamellar ridge*-Pt-1, *inverse-V ridge*-Pt-2 and *ridge/nano-hole*-Pt-2, respectively. First, these wing samples were cleaned in absolute ethanol, with unrelated scales carefully removed by a cotton swab, leaving the required scales for further architectured Pt preparation. The flat wing membrane of *Morph* and *Troides aeacus* butterfly with all scales removed was also prepared and cleaned with the same procedure as the unarchitectured Pt(*flat*-Pt-1 and *flat*-Pt-2) template.

***Surface functionalizing-electroless deposition*:** See reference 1 for detailed processes and parameters.[1] After surface functionalizing and electroless deposition, the Pt-coated scales were removed from the membrane and collected for further detemplating process for architectured Pt. The Pt-coated membrane was collected for unarchitectured Pt.

***Detemplating*:** The as-prepared Pt-coated scales and Pt-coated membrane were rinsed in phosphoric acid at room temperature for 72 h to remove the bio-templates. These samples were then further washed by absolute ethanol and collected by centrifugation for several times and dried at 60℃ for 12 h before finally obtaining the architectured Pt and unarchitectured Pt samples.

S2. Finite element simulation process

To investigate the architecture effect on methanol transport, we conducted finite element modeling and simulating using Comsol Multiphysics 4.2 software from CnTech. A diffusion domain approach with a one-ridge period as a domain unit was used.[2] Both outer and inner catalytic surfaces of lamellar ridges were investigated, as well as an unarchitectured counterpart with an ideal flat surface.

Equation (1) shows the methanol oxidation process investigated in this work:

$$CH_3OH + H_2O \rightarrow CO_2 + 6H^+ + 6e^- \qquad (1)$$

Methanol oxidation is a zero-order reaction when the methanol concentration is higher than 0.1M.[3,4] In this work, we used the Tafel kinetic equation developed by Ren *el al.*[5] as the boundary condition on the electrocatalyst surface.

$$I = I_0^{CH3OH}\, exp\left(\frac{\alpha_a F}{RT}\eta_a\right) \qquad (2)$$

$$N^{CH3OH} = \frac{I}{F} \qquad (3)$$

Where I is the current density; η_a is the overpotential. I_0^{CH3OH} as the exchange current density, and α_a as the charge transfer coefficient is considered to be catalyst dependent and varies in different catalytic systems.[3-9] Here, we used the referenced value of 0.23 and 10.07 A/m^2 at 25℃ for α_a and I_0^{CH3OH} respectively.[3-5] N^{CH3OH} is the diffusion flux for methanol on the electrocatalyst surface.

The mass transport of methanol is described by Fick's Second Law of Diffusion neglecting convection and migration as follows:

$$\frac{\partial C}{\partial t} = D\left(\frac{\partial^2 C}{\partial x^2} + \frac{\partial^2 C}{\partial y^2} + \frac{\partial^2 C}{\partial z^2}\right) \qquad (4)$$

Where C is methanol concentration; t is time; D is diffusion coefficient of methanol in liquid electrolyte with a value of 1.69x10^{-9} m^2/s.[4]

The bulk solution condition is implemented at a distance of $6\sqrt{\tau}$ from the highest point of the electrode. Beyond this, the effects of diffusion are not important on the given time scale.[2] Here, τ is a calculated distance obtained by the multiplication of the diffusion coefficient and time needed for the electrochemical process. Periodic conditions were set at the periodic diffusion domain border. An equilibrium potential (η_a=0, $N = I_0^{CH3OH}/F$) was applied to analyze the reactant diffusion behavior for architectured and unarchitectured catalysts.

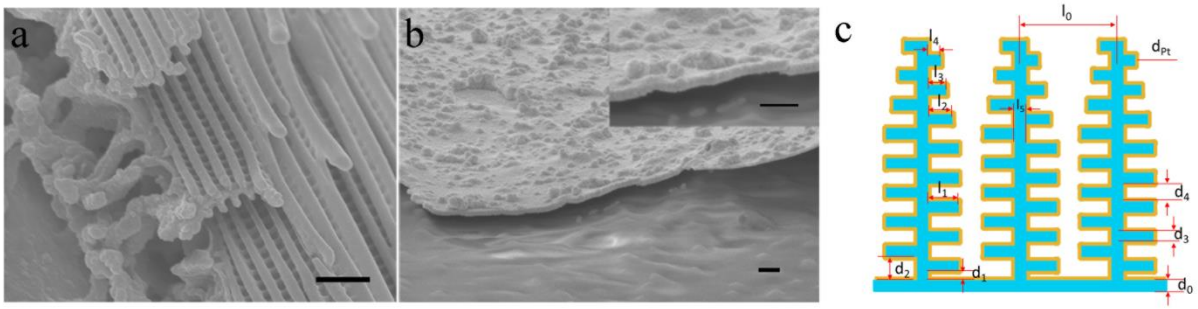

Fig. S1. (a,b) FESEM images showing the side view of original lamellar-ridge architectured scale and *flat*-Pt-1, respectively. Scale bar: 500 nm for both. (c) Comsol Multiphysics modeling for lamellar-ridge architecture with dimensional parameters. Blue: original template (removed). Orange: Pt coating. (See Table S1 for detailed parameters)

Fig. S2. Digital photograph of a *Troides aeacus* butterfly. Scale bar: 1cm.

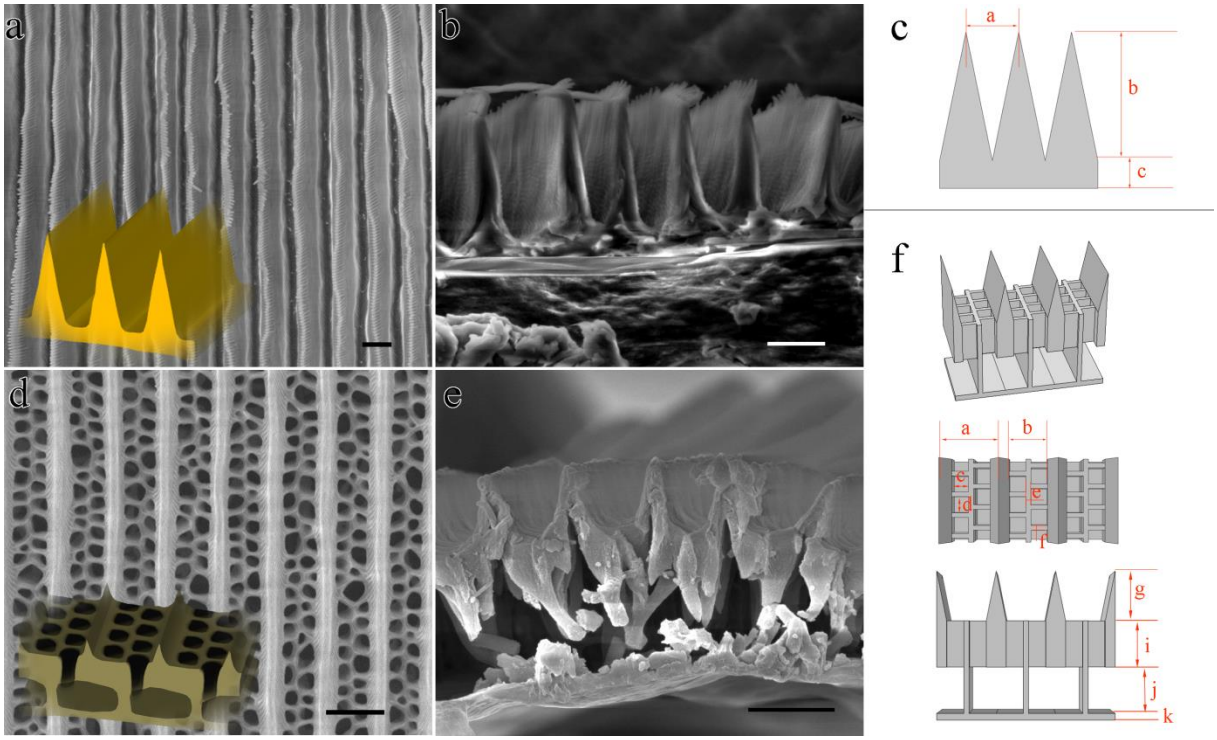

Fig. S3. Microarchitectures of original *Troides aeacus* butterfly wing scales depicted by FESEM images. (a,b) Front and cross-sectional views of yellow hind-wing scale with inverse-V type ridge architecture. (c) COMSOL Multiphysics model and dimensional parameters for inverse-V ridge architecture. (d,e) Front and cross-sectional views of black fore-wing scale with ridge/nano-hole array architecture. (f) COMSOL Multiphysics model and dimensional parameters for ridge/nano-hole architecture. Scale bar: 2μm for all. (See Table S2,S3 for detailed parameters)

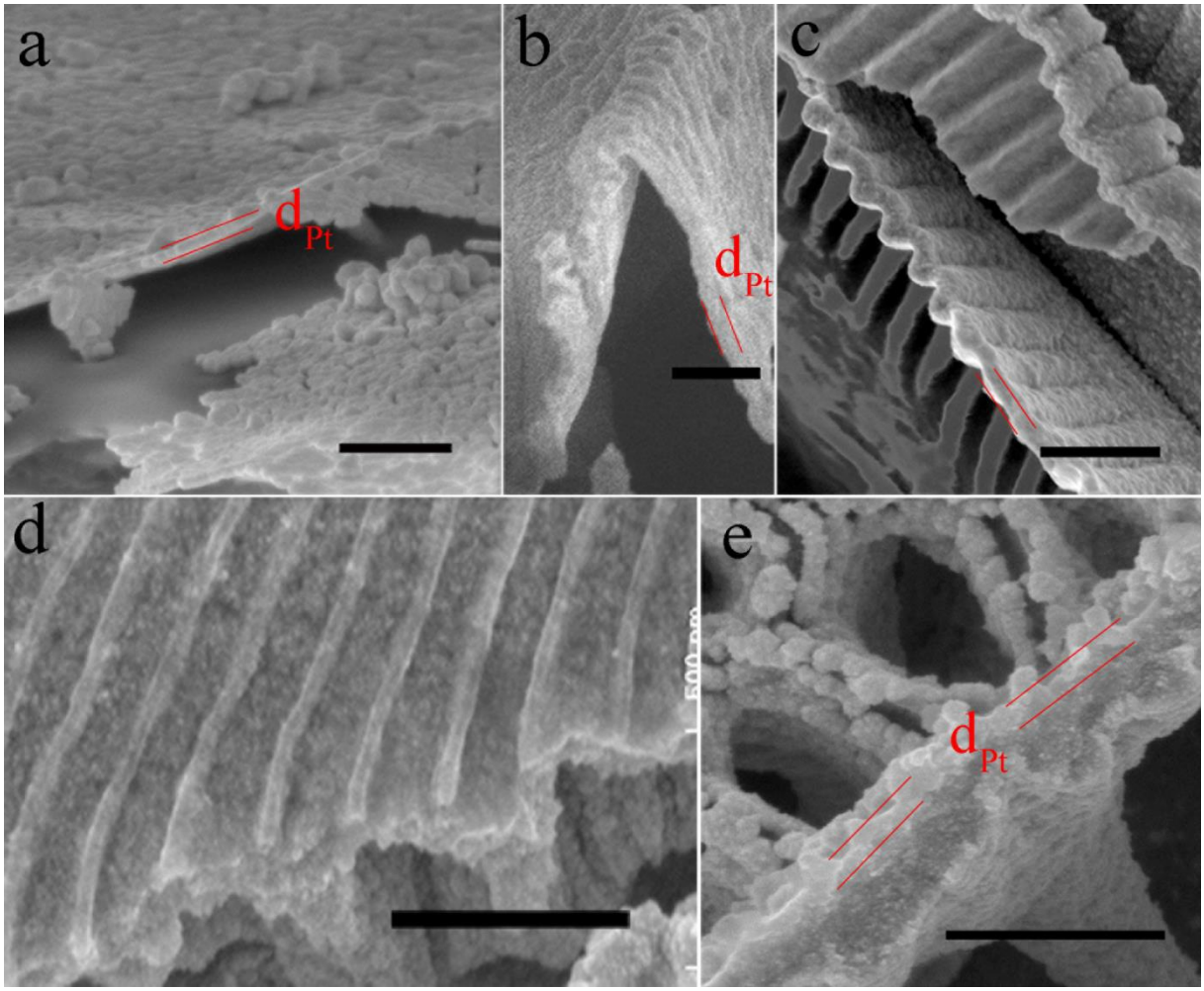

Fig. S4. FESEM images showing the cross-sectional views of (a) *flat*-Pt-2; (b,c) *inverse-V ridge*-Pt-2; and (d,e) *ridge/nano-hole*-Pt-2. Scale bar: 500nm for all.

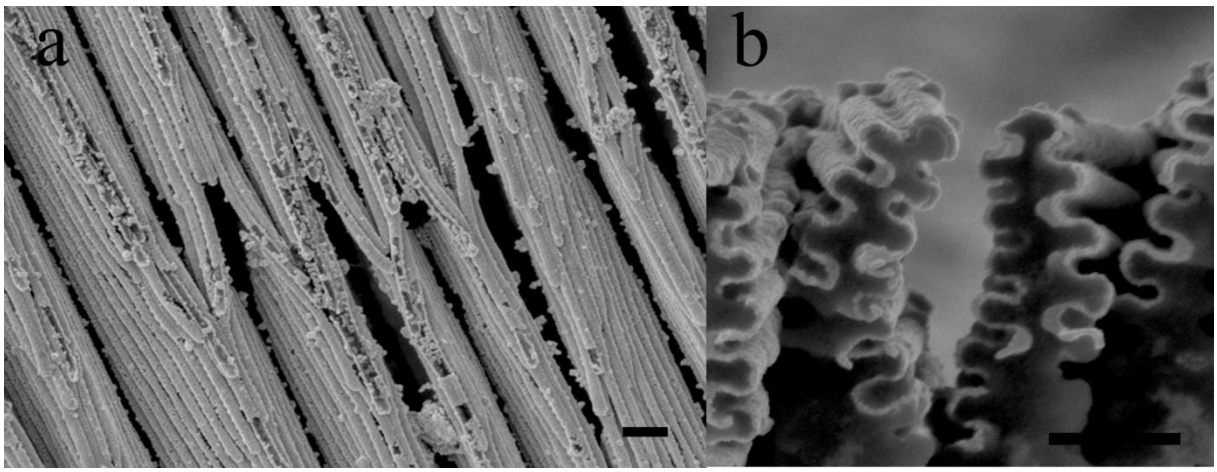

Fig. S5. FESEM images of *lamella ridge*-Pt-1 after 100 voltammetric cycles. (a) The front view. (b) The cross sectional view.

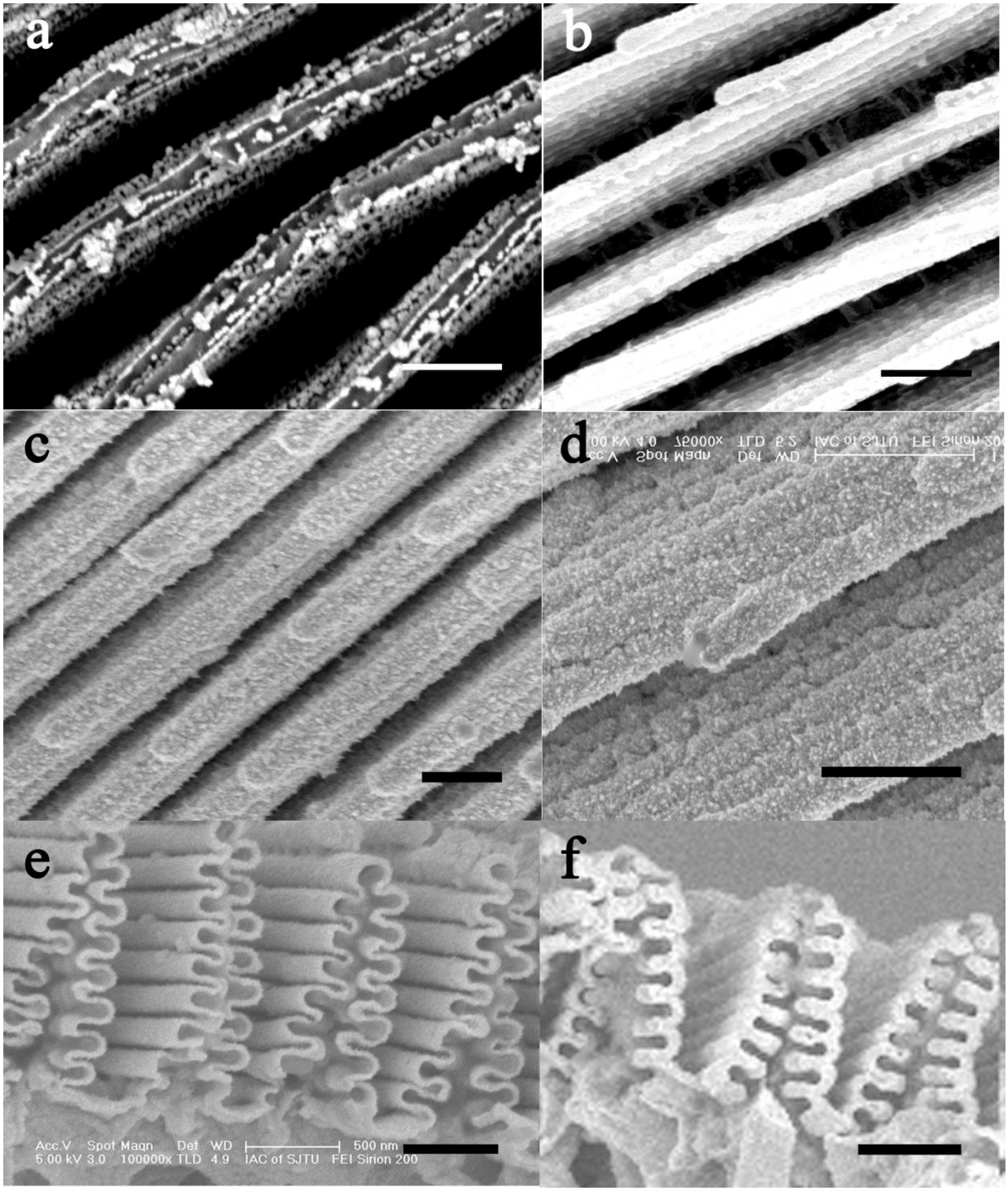

Fig. S6. FESEM images of *lamellar ridge*-Pt-1 samples fabricated under different electroless deposition time. (a) 2h, (b) 2h 30min, (c,e) 3h, (d,f) 3h 30min.

Table S1 Dimensions for modeling of *lamellar ridge*-Pt-1 (Fig. S1)

l_0(nm)	l_1(nm)	l_2(nm)	l_3(nm)	l_4(nm)	l_5(nm)	d_0(nm)	d_1(nm)	d_2(nm)	d_3(nm)	d_4(nm)	d_{Pt}(nm)
650	243	200	160	120	80	80	60	157.5	75	120	26

Table S2 Dimensions for modeling of *inverse-V ridge*-Pt-2 (Fig. S3,S4)

a(μm)	b(μm)	c(μm)	d_{Pt}(nm)
2.3	5.6	1.2	98

Table S3 Dimensions for modeling of *ridge/nano-hole*-Pt-2 (Fig. S3,S4)

a(μm)	b(μm)	c(μm)	d(μm)	e(μm)	f(μm)	g(μm)	i(μm)	j(μm)	k(μm)	d_{Pt}(nm)
1.8	1.2	0.52	0.49	0.16	0.14	1.5	1.4	1.4	0.2	81

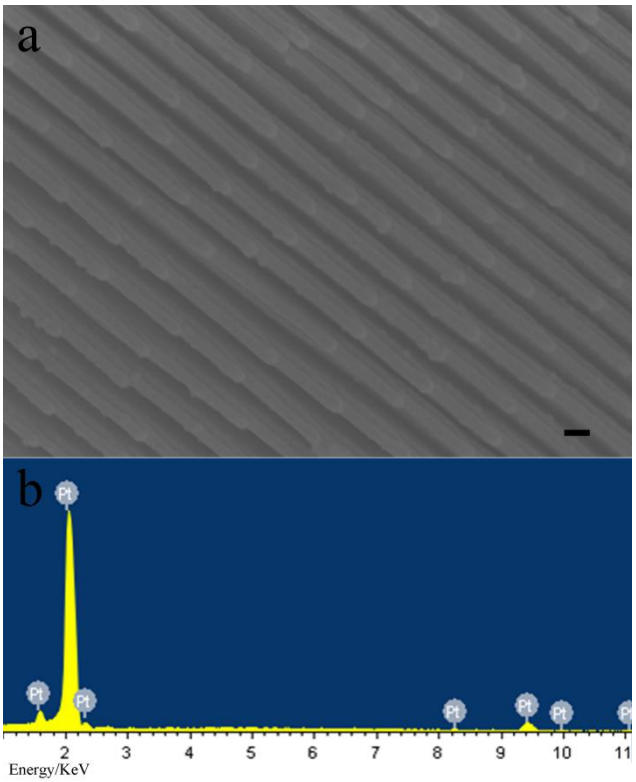

Fig. S7. (a) FESEM image of *lamellar ridge*-Pt-1 and (b) corresponding EDS.

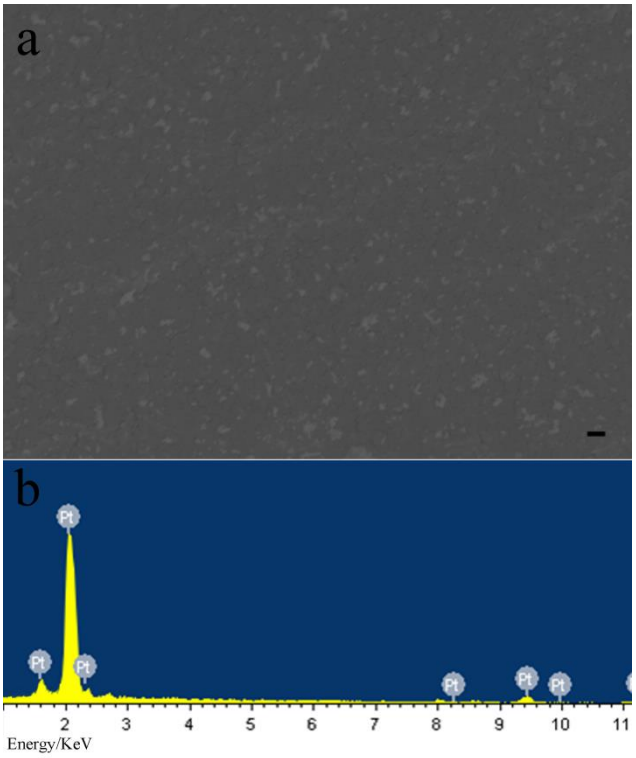

Fig. S8. (a) FESEM image of *flat*-Pt-1 and (b) corresponding EDS.

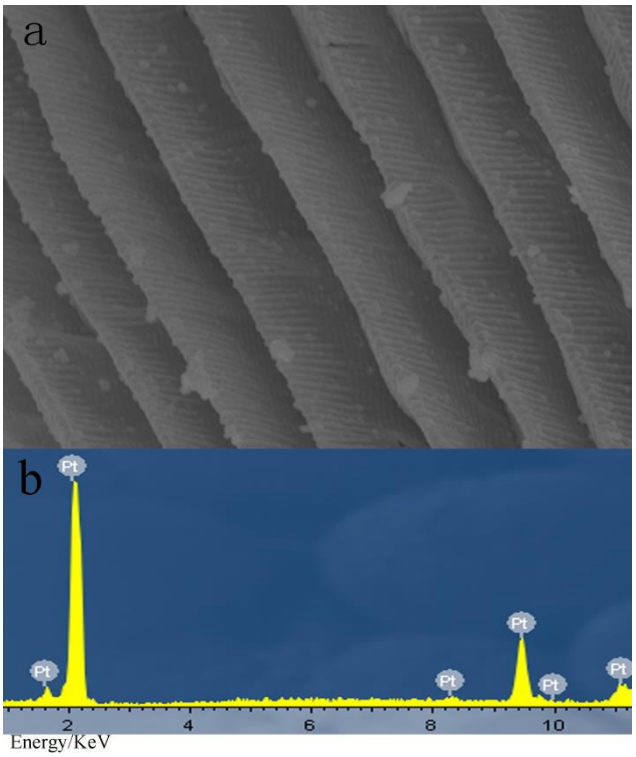

Fig. S9. (a) FESEM image of *inverse-V ridge*-Pt-2 and (b) corresponding EDS.

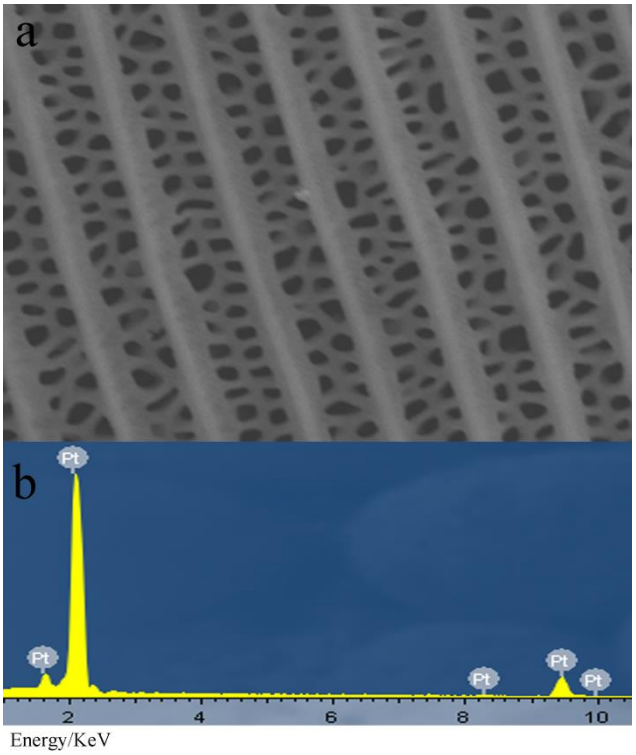

Fig. S10. (a) FESEM image of *ridge/nano-hole-array*-Pt-2 and (b) corresponding EDS.

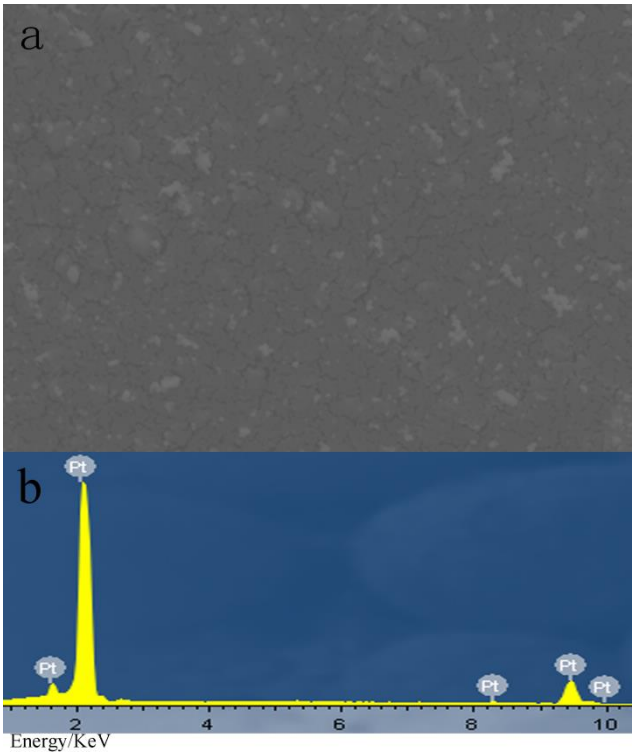

Fig. S11. (a) FESEM image of *flat*-Pt-2 and (b) corresponding EDS.

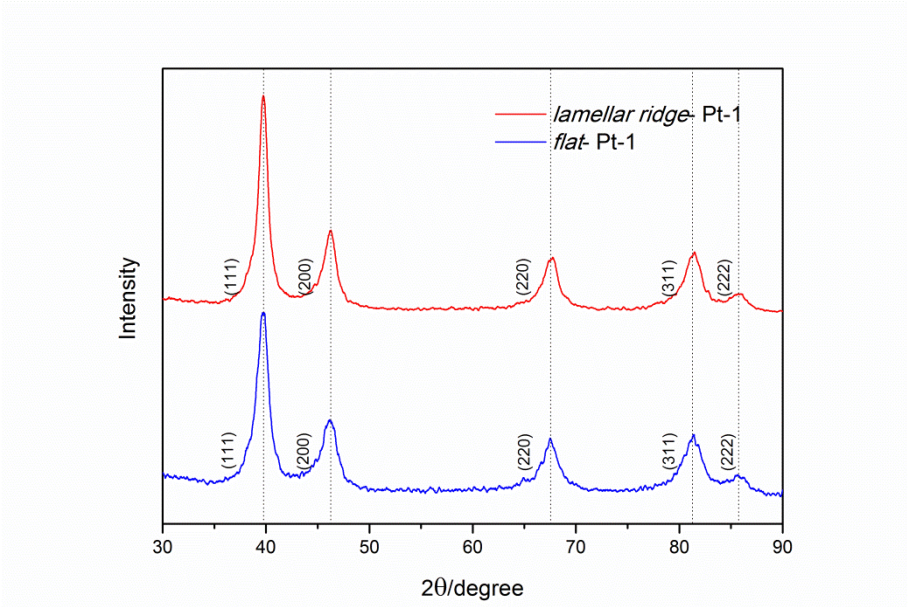

Fig. S12. X-ray diffraction patterns of *lamellar ridge*-Pt-1 and *flat*-Pt-1 samples.

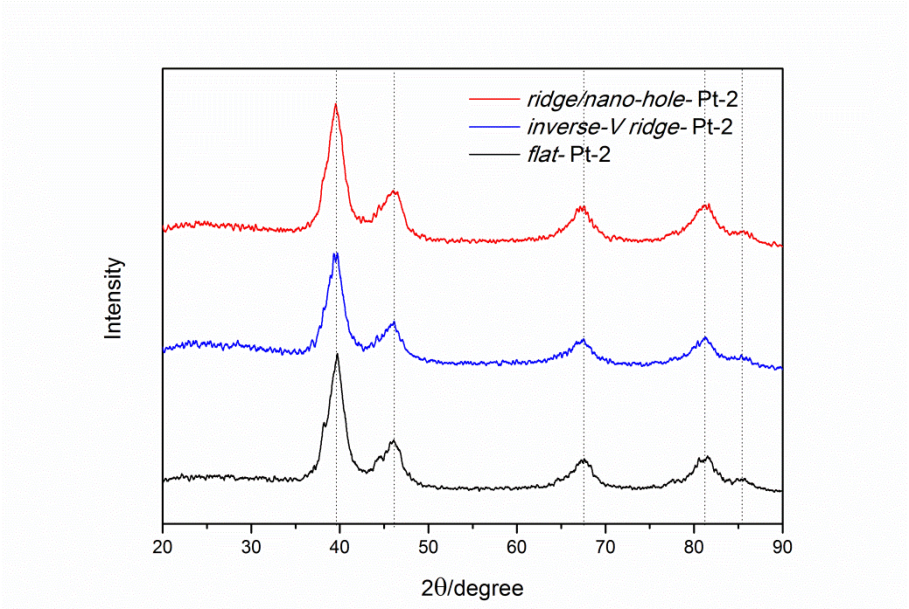

Fig. S13. X-ray diffraction patterns of *inverse-V ridge*-Pt-2 , *ridge/nano-hole*-Pt-2 and *flat*-Pt-2 samples.

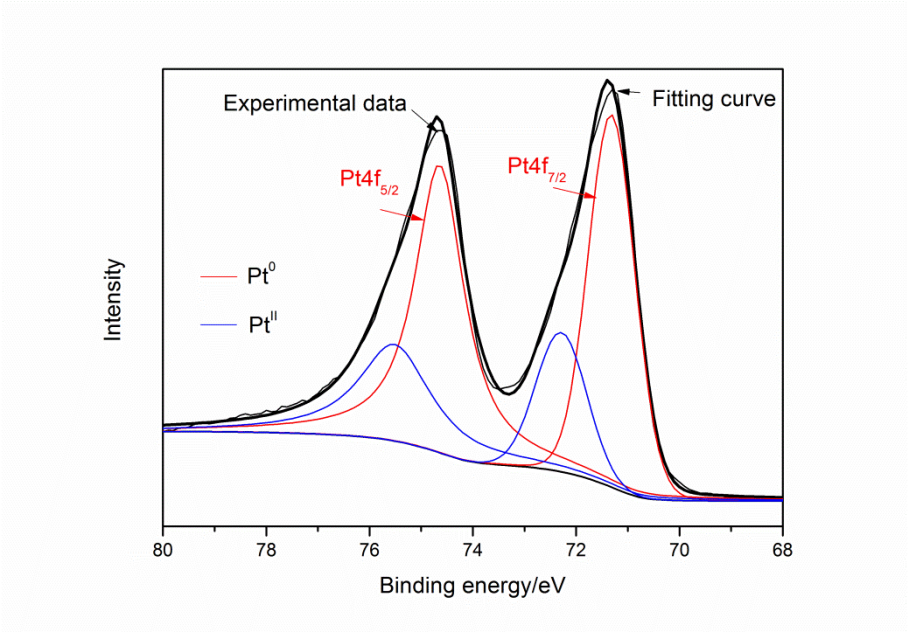

Fig.S14. XPS spectrum of *lamellar ridge*-Pt-1 after detemplation.

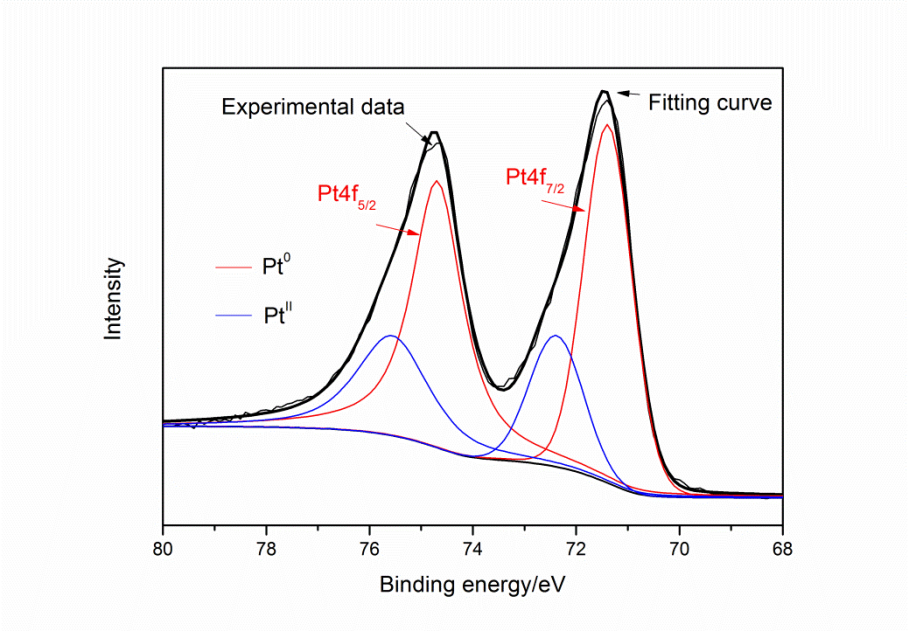

Fig.S15. XPS spectrum of *flat*-Pt-1 after detemplation.

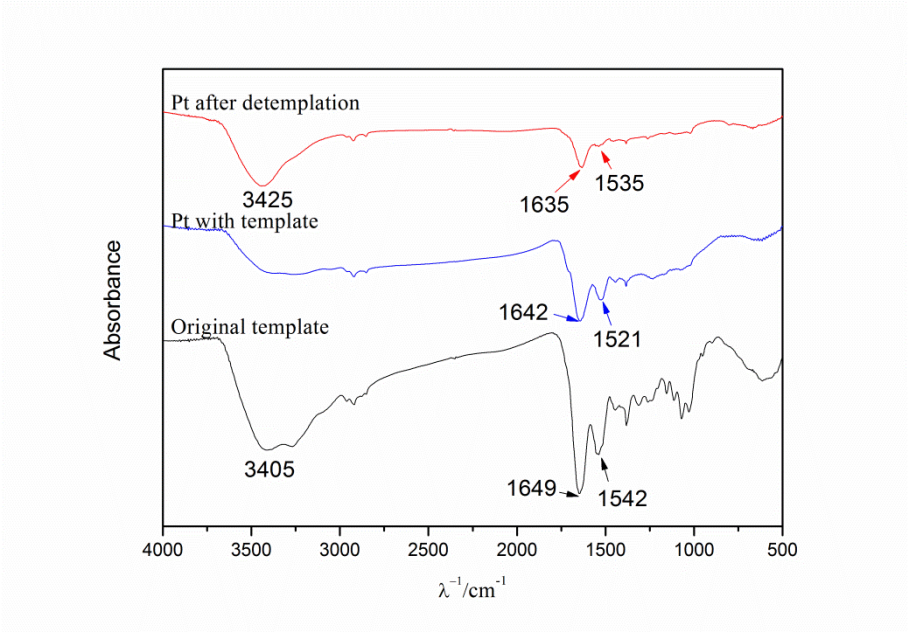

Fig. S16. FTIR spectra of original butterfly wing template, Pt with template, and Pt after detemplation .

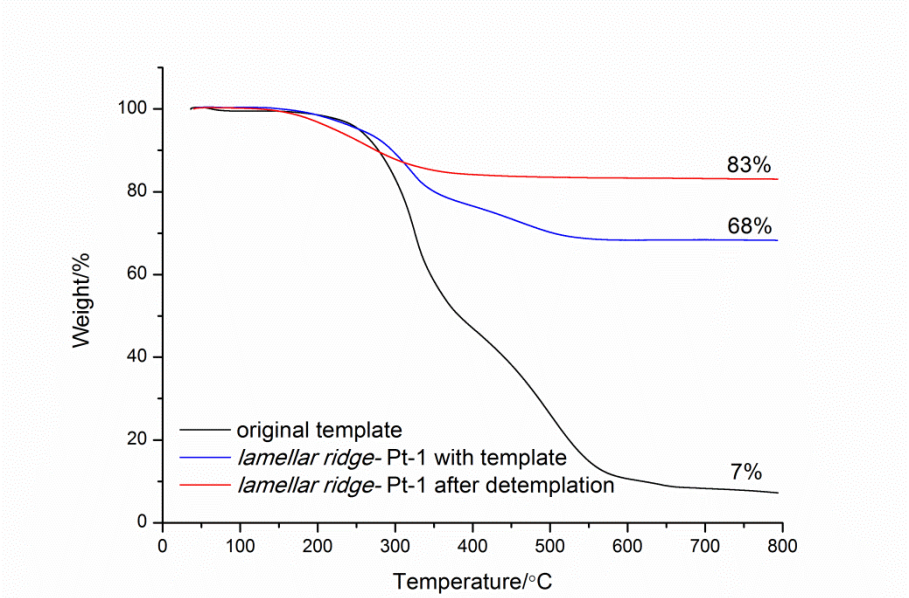

Fig. S17. Thermal gravimetric analysis (TGA) for original wing template, and *lamellar ridge*-Pt-1 before and after detemplation.

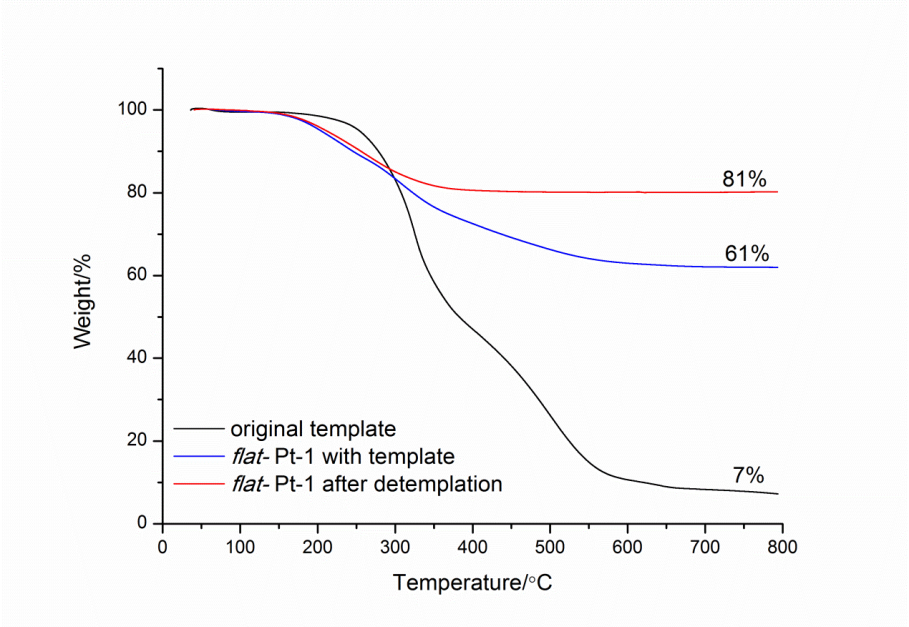

Fig. S18. Thermal gravimetric analysis (TGA) for original wing template, and *flat*-Pt-1 before and after detemplation.

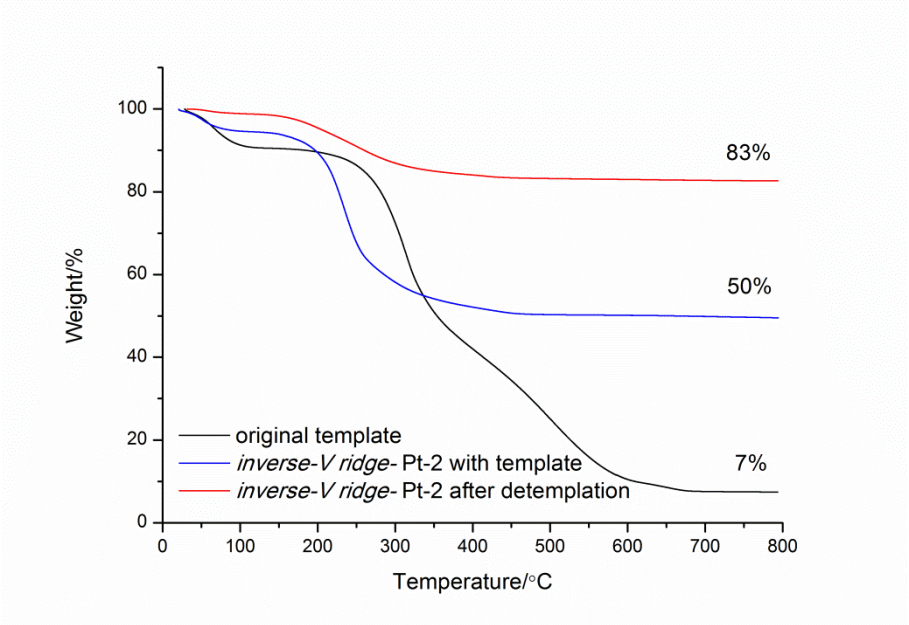

Fig. S19. Thermal gravimetric analysis (TGA) for original wing template, and *inverse-V ridge*-Pt-2 before and after detemplation.

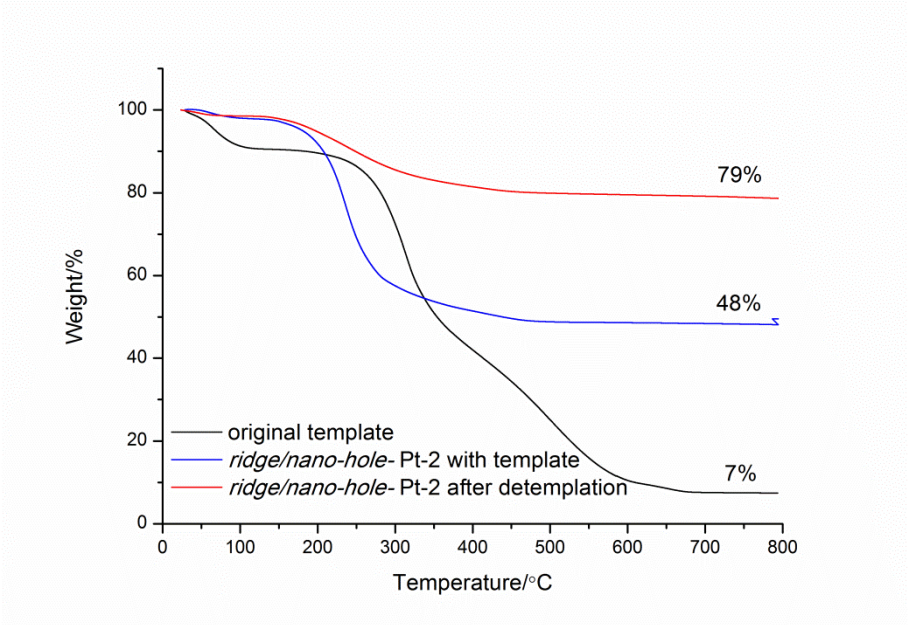

Fig. S20. Thermal gravimetric analysis (TGA) for original wing template, and *ridge/nano-hole*-Pt-2 before and after detemplation.

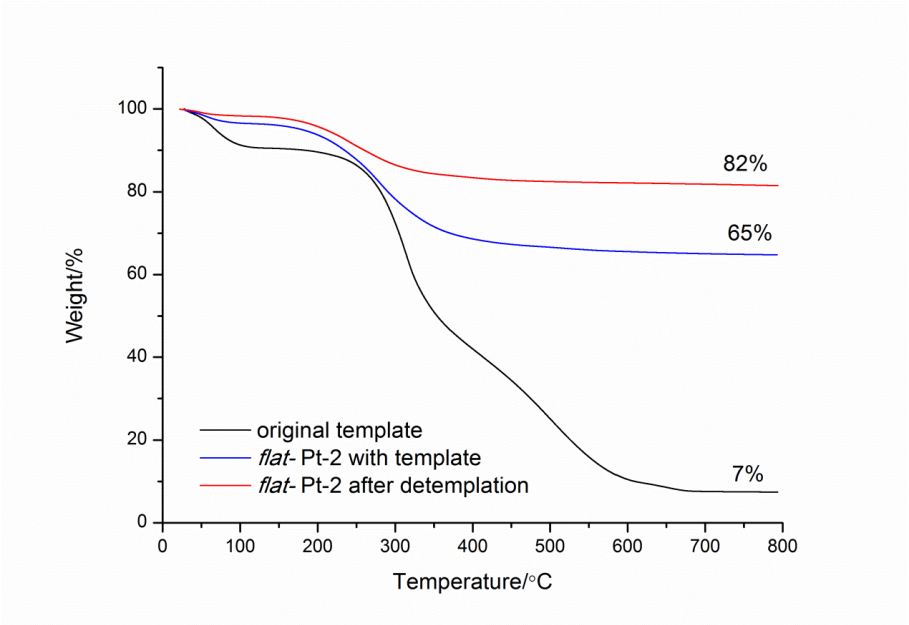

Fig. S21. Thermal gravimetric analysis (TGA) for original wing template, and *flat*-Pt-2 before and after detemplation.

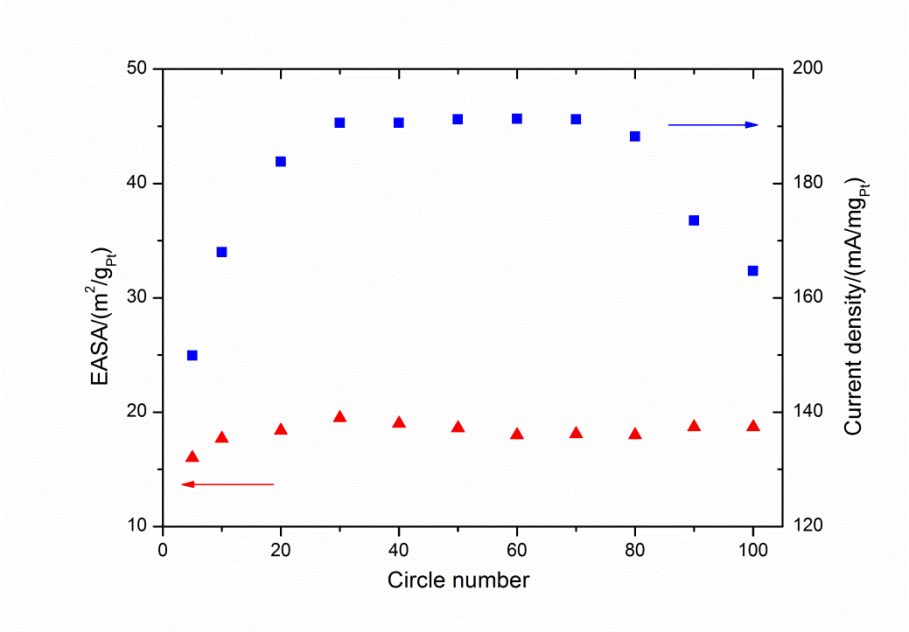

Fig. S22. Variation of *EASA* (red) and I_f (blue) for *lamellar ridge*-Pt-1 as a function of the cycle number. Scan rate: 50mV/s.

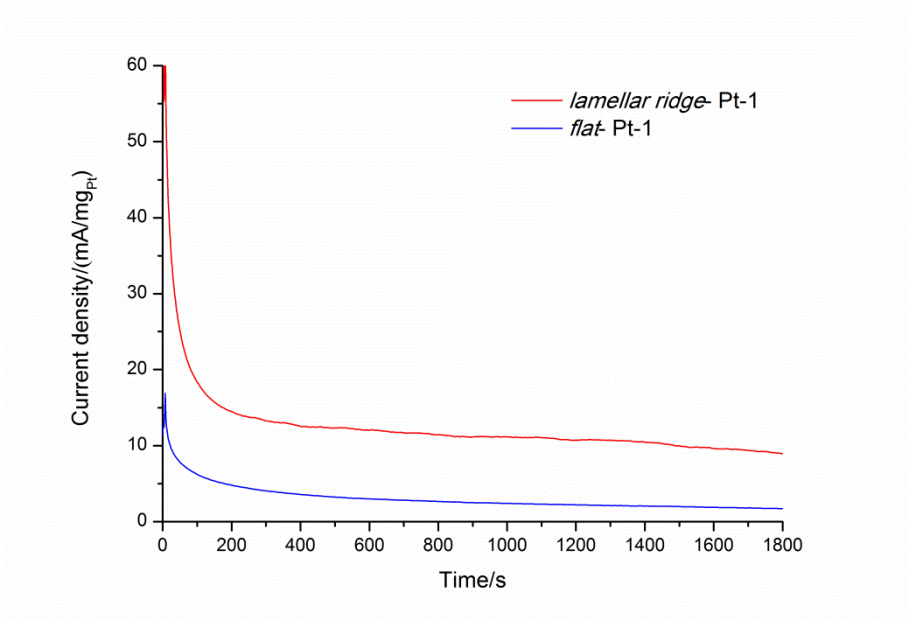

Fig. S23. Chronoamperometry curves for *lamellar ridge*-Pt-1 and *flat*-Pt-1 at 0.5 V(vs. SCE) in an aqueous solution of 1 M CH_3OH and 0.5 M H_2SO_4.

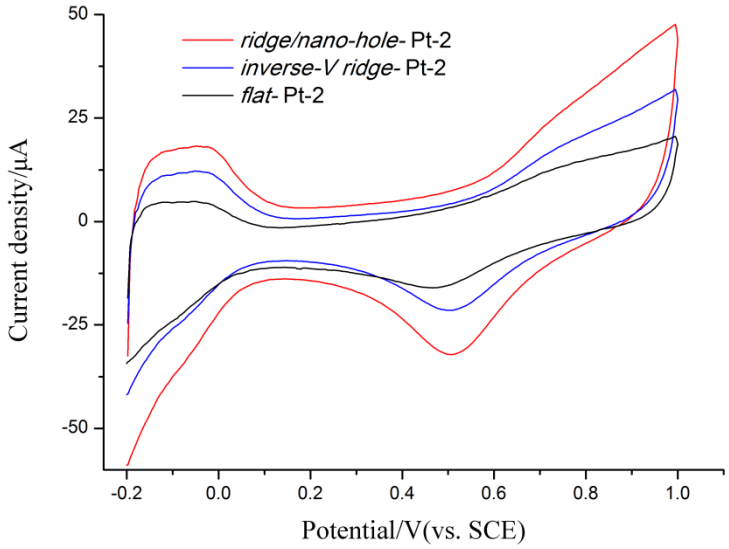

Fig. S24. Cyclic voltammograms for *inverse-V ridge*-Pt-2, *ridge/nano-hole*-Pt-2, and *flat*-Pt-2 at 50mV/s in an aqueous solution of 0.5 M H_2SO_4.

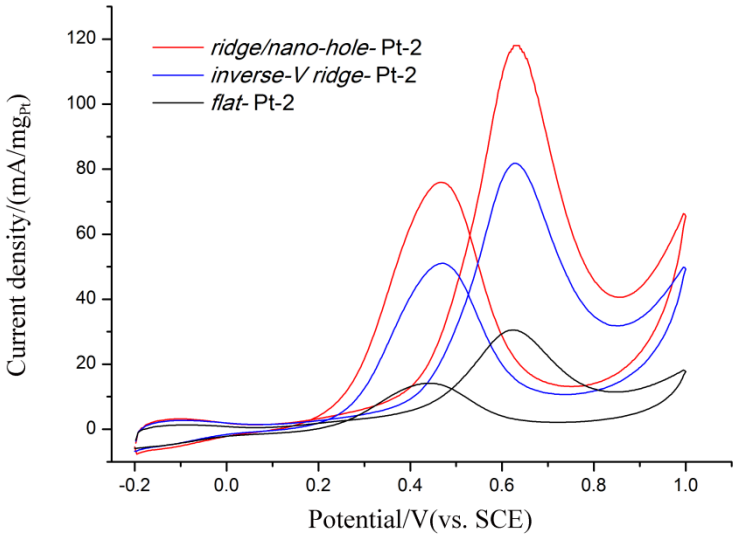

Fig. S25. Cyclic voltammograms for *inverse-V ridge*-Pt-2, *ridge/nano-hole*-Pt-2, and *flat*-Pt-2 at 50mV/s in an aqueous solution of 1 M CH_3OH and 0.5 M H_2SO_4.

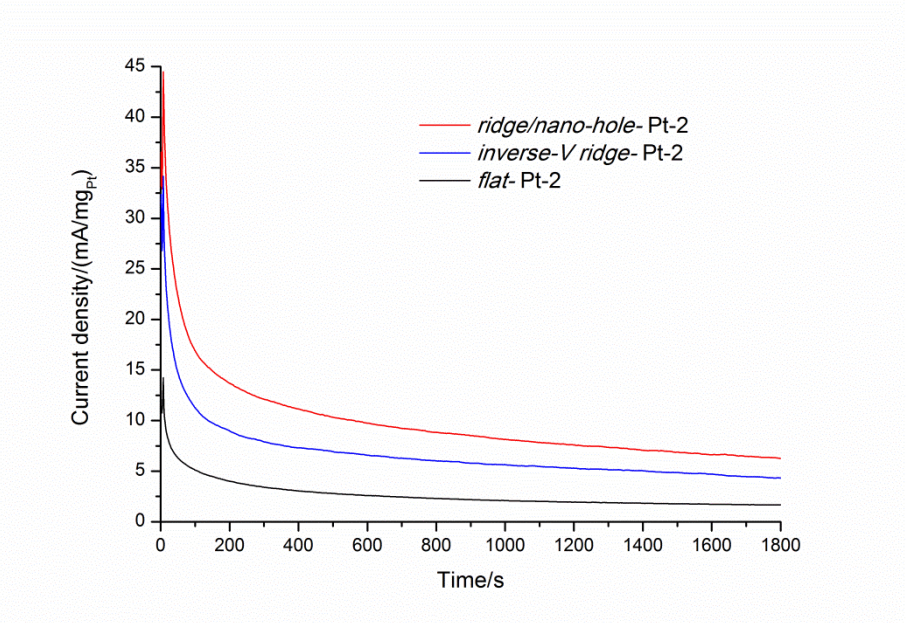

Fig. S26. Chronoamperometry curves for *inverse-V ridge*-Pt-2, *ridge/nano-hole*-Pt-2, and *flat*-Pt-2 at 0.5 V(vs. SCE) in an aqueous solution of 1 M CH_3OH and 0.5 M H_2SO_4.

Table S4 Forward peak potential of methanol oxidation voltammograms for all samples.

Samples	*flat*-Pt-1	*lamella ridge*-Pt-1	*flat*-Pt-2	*inverse-V ridge*-Pt-2	*ridge/nano-hole*-Pt-2
Peak potenial/ mV(vs. SCE)	626	628	626	*628*	631

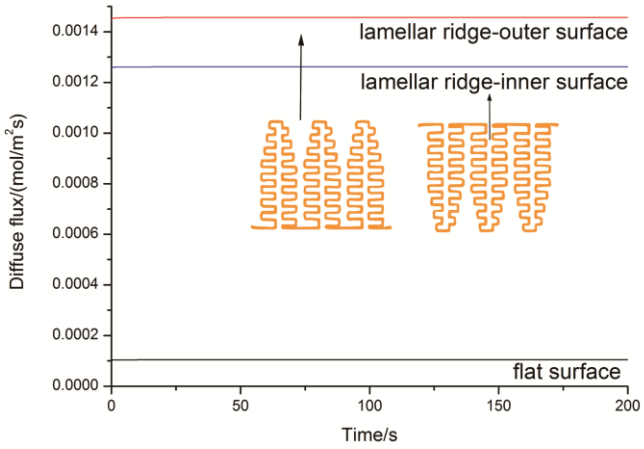

Fig. S27. Calculated methanol diffusion flux for outer and inner surface models of lamellar-ridge architecture and their unarchitectured counterpart under equilibrium potential.

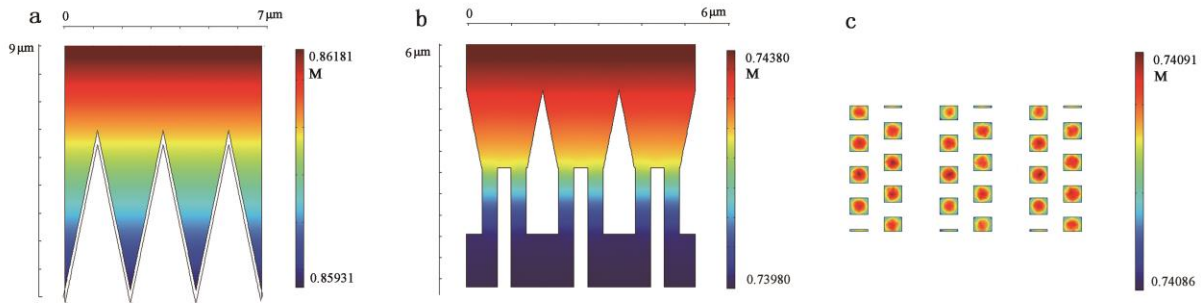

Fig. S28. Reactant concentration profiles at t=100s in the simulating process at electrocatalyst architectures and local bulk solution for inverse-V ridge architectured model(a), and vertical and parallel cross-section of ridge/nano-hole array architectured model(b,c).

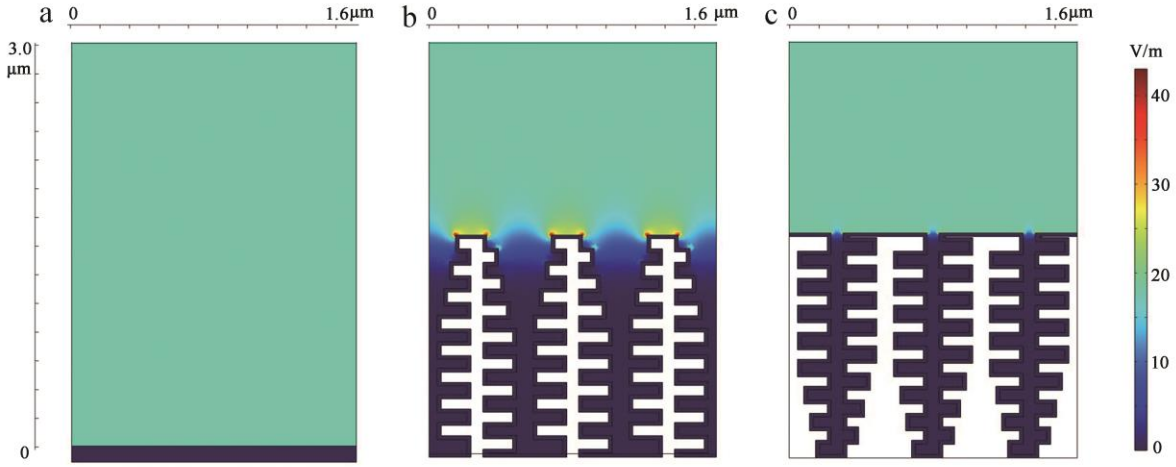

Fig. S29. Simulated electric field intensity(*E*) distribution at electrocatalyst architectures and local bulk solution for unarchitectured model(a), outer surface model of lamellar ridge architecture(b), and inner surface model of lamellar-ridge architecture(c). A constant potential (0.1V) was exerted on the three models, while a zero potential boundary condition was applied at an assumed semi-diffusion distance (5mm) at the Electrostatics branch under AC/DC Module of COMSOL Multiphysics software. Electrode material was defined as metal platinum, while the relative dielectric constant of liquid electrolyte was set to 81. The constitutive relation was defined by Gauss' law in the whole domain.

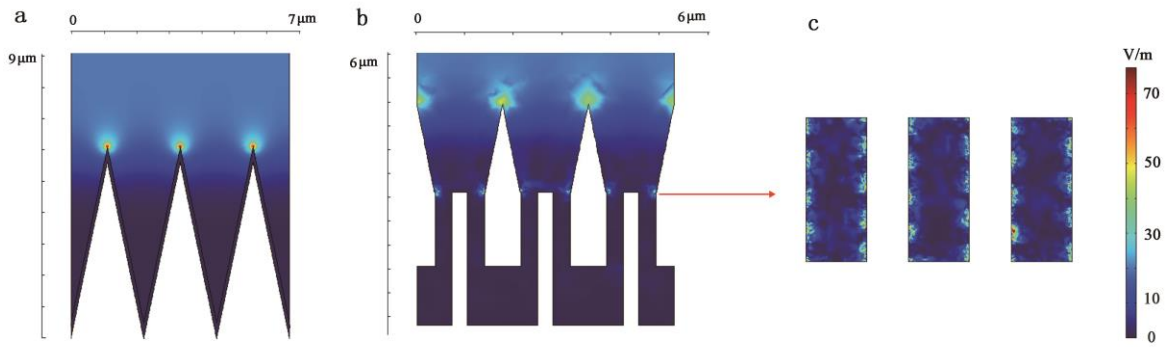

Fig. S30. Simulated electric field intensity(*E*) distribution at electrocatalyst architectures and local bulk solution for inverse-V ridge model (a), and vertical and parallel cross-section of ridge/nano-hole array model (b,c).

References

1 Y. Tan, J. Gu, X. Zang, W. Xu, K. Shi, L. Xu and D. Zhang, *Angew. Chem.,* 2011, **123**, 8457-8461.

2 D. Menshykau, I. Streeter and R. G. Compton, *J. Phys. Chem. C.,* 2008, **112**, 14428-14438.

3 X. Ren, P. Zelenay, S. Thomas, J. Davey and S. Gottesfeld, *J. Power Sources,* 2000, **86**, 111-116.

4 Z. H. Wang and C. Y. Wang, *J. Electrochem. Soc.,* 2003, **150**, A508-A519.

5 P. S. Kauranen and E. Skou, *J. Electroanal. Chem.,* 1996, **408**, 189-198.

6 J. Nordlund and G. Lindbergh, *J. Electrochem. Soc.,* 2002, **149**, A1107-A1113.

7 C. H. Chen and T. K. Yeh, *J. Power Sources,* 2006, **160**, 1131-1141.

8 S. F. Baxter, V. S. Battaglia and R. E. White, *J. Electrochem. Soc.,* 1999, **146**, 437- 447.

9 B. L. Garcia, V. A. Sethuraman, J. W. Weidner and R. E. White, *J. Fuel Cell Sci. Tech.,* 2004, **1**, 43-48.